The influence of Reynolds number on a plane jet

Ravinesh C. Deo,[a] Jianchun Mi,[b] and Graham J. Nathan
Fluid Mechanics, Energy and Combustion Group, School of Mechanical Engineering, The University of Adelaide, South Australia 5005, Australia

(Received 31 January 2008; accepted 17 June 2008; published online 22 July 2008)

The present study systematically investigates through experiments the influence of Reynolds number on a plane jet issuing from a radially contoured, rectangular slot nozzle of large aspect ratio. Detailed velocity measurements were performed for a jet exit Reynolds number spanning the range $1500 \leq \mathrm{Re}_h \leq 16\,500$, where $\mathrm{Re}_h \equiv U_b h/\nu$ with U_b as the momentum-averaged exit mean velocity, h as the slot height, and ν as the kinematic viscosity. Additional centerline measurements were also performed for jets from two different nozzles in the same facility to achieve $\mathrm{Re}_h = 57\,500$. All measurements were conducted using single hot-wire anemometry to an axial distance (x) of $x \leq 160h$. These measurements revealed a significant dependence of the exit and the downstream flows on Re_h despite all exit velocity profiles closely approximating a "top-hat" shape. The effect of Re_h on both the mean and turbulent fields is substantial for $\mathrm{Re}_h < 10\,000$ but becomes weaker with increasing Re_h. The length of the jet's potential core, initial primary-vortex shedding frequency, and far-field rates of decay and spread all depend on Re_h. The local Reynolds number, $\mathrm{Re}_{y0.5} \equiv 2U_c y_{0.5}/\nu$, where U_c and $y_{0.5}$ are the local centerline velocity and half-width, respectively, are found to scale as $\mathrm{Re}_{y0.5} \sim x^{1/2}$. It is also shown that, for $\mathrm{Re}_h \geq 1500$, self-preserving relations of both the turbulence dissipation rate (ε) and smallest scale (η), i.e., $\varepsilon \sim \mathrm{Re}_h^3 (x/h)^{-5/2}$ and $\eta \sim \mathrm{Re}_h^{-3/4} (x/h)^{5/8}$, become valid for $x/h \geq 20$. © *2008 American Institute of Physics*.
[DOI: 10.1063/1.2959171]

I. INTRODUCTION

Following the early investigation of Schlichting,[1] plane jets have received significant attention from the turbulence research community.[2–10] A practical plane jet is produced by a rectangular slot of dimensions $w \times h$, with $w \gg h$ (where w and h are the slot's long and short sides) bounded by two parallel plates, known as sidewalls, attached to the slot's short sides. The presence of sidewalls restrict the jet from developing in the direction normal to the short sides, so that the flow develops statistically two dimensionally up to a certain downstream distance, provided that the nozzle aspect ratio, $\mathrm{AR}(\equiv w/h)$, is sufficiently large.[11] The primary objective of the present work is to investigate the effect of Reynolds numbers on the downstream development of a plane jet.

Studies undertaken over many years[12–16] have shown that the downstream development of a jet depends on the flow at the jet origin, often termed initial conditions. The analytical work of George[12] and experimental assessments on round and plane jets (e.g., Refs. 13–16) pointed out that their asymptotic states depend on the initial conditions. The initial conditions of a jet are conventionally defined to be the exit Reynolds number (Re_h), nature of exit lateral profiles of mean velocity and turbulence intensity, aspect ratio (AR) (noncircular jets), nozzle-exit geometric profiles, and global density ratio of the jet fluid to ambient fluid. The downstream development of a jet is also dependent on the boundary conditions, e.g., the presence or absence of sidewalls for a plane jet. In our previous work on a plane jet, we have characterized the effects of AR,[11] nozzle geometric profile,[16] and the sidewalls.[17] Some insight into the effects of Re_h on a plane jet can be gleaned from the limited investigations reviewed below. However, no detailed assessment of this influence in both the near and far fields is available. The present work aims to fulfill this need.

The influence of Reynolds number on a jet's development is challenging to understand. This is partly because the Reynolds number affects the development of the boundary layer through the nozzle, making it difficult to independently assess jet development and exit boundary layer thickness. Zaman[18] found that the initial turbulence intensity and boundary layer growth of a round jet are functions of jet exit Reynolds number (Re_d). His work showed that round jets are initially laminar when measured at $\mathrm{Re}_d < 1.0 \times 10^5$ but become fully turbulent when $\mathrm{Re}_d > 5.0 \times 10^5$. Hence Reynolds numbers exerts both a direct influence on the turbulent mixing field by controlling the significance of viscosity and an indirect influence by modifying the initial conditions (e.g., boundary layer thickness).

It is well known that at sufficiently high Reynolds number, the jet decay and spread rates of round jets are almost independent of Re.[19,20] However, there is some variation in the reported values of jet exit Reynolds number at which this occurs, suggesting that it depends on initial conditions. In a

[a]Present address: The Center for Remote Sensing and Spatial Information Sciences, School of Geographical Sciences and Planning, The University of Queensland, Brisbane 4072, Australia.
[b]Author to whom correspondence should be addressed. Also at Department of Energy and Resource Engineering, College of Engineering, Peking University, Beijing 100871, China. Electronic mail: jcmi@coe.pku.edu.cn. Telephone: +86 10 6276 7074.

related review for round jets, Dimotakis[21] concluded that a fully developed turbulent field occurs when $Re_d \geq 10^4$. The experimental work of Dimotakis *et al.*,[22] which assessed the scalar-mixing fields of round jets at $Re_d = 2.5 \times 10^3$ and 10^4, found the asymptotic state to occur for $Re_d = 10^4$. Miller and Dimotakis[23] reported that the scalar fluctuations decrease with an increase in Re_d and converge to an asymptotic state for $Re_d \approx 2.0 \times 10^4$. Likewise, Gilbrech[24] found that the asymptotic state of the mixing field occurs near $Re_d \approx 2.0 \times 10^4$. Koochesfahani and Dimotakis[25] used scalar images of laser-induced fluorescence at $Re_d = 1.75 \times 10^3$ and 2.30×10^4 to show more qualitative and well-mixed state at $Re_d = 2.30 \times 10^4$ relative to $Re_d = 1.75 \times 10^3$. Similar results were found by Michalke,[26] who found that the growth of instability waves in jet shear layers can be reduced dramatically when the Reynolds number is increased sufficiently.

Oosthuizen[27] measured the flow of a round jet at low Reynolds number and found that both the mean and turbulence fields depend strongly on Re_d for $Re_d < 10^4$. Bogey and Bailly[28] used large eddy simulations of a transitional round jet ($1.70 \times 10^3 \leq Re_d \leq 4.0 \times 10^5$) and showed that as Re_d decreases, a jet develops more slowly within the potential core, but more rapidly further downstream. Their round jets achieved self-similarity closer to the exit plane at low values of Re_h, a finding, which agrees well with Pitts[29] for turbulent axisymmetric jets measured between $3950 \leq Re_d \leq 11\,880$. Moreover, Mi *et al.*[14] found that the scalar decay rate in the self-similar far field depends strongly on Re_d when the jet issues from a smooth contraction, but this dependence becomes much weaker and may be negligible for jets originating from a long pipe, in which the flow is fully turbulent.

Less detail is available for the transition to an asymptotic state for a plane jet. The investigation by Lemieux and Oosthuizen[30] over the range $700 \leq Re_h \leq 4200$ found a significant influence of Re_h on the shear stress, jet decay, spreading rates, and mean velocity profiles. While their study concluded that jet properties become invariant of Re_h for $Re_h > 4200$, other investigations have found a different Re_h threshold for this invariance. Namar and Ötügen,[31] who measured a high-AR rectangular jet over the range $1000 \leq Re_h \leq 7000$, showed that Re_h has significant influence on the mixing field for $Re_h \leq 7000$. Likewise, Everitt and Robbins,[32] whose measurements for a plane jet spanned $1.6 \times 10^4 \leq Re_h \leq 7.5 \times 10^4$, reported a large spread in velocity decay rates. However, it is not possible to separate the effects of Re_h from AR in their investigation since this was also varied between AR=21 and AR=128.[11] Klein *et al.*[33] conducted a direct numerical simulation (DNS) investigation of a plane jet in the near and transition fields (i.e., for $x/h \leq 20$) but for lower ranges of Reynolds numbers, $Re_h \leq 6000$. It is evident that none of these investigations reached the range $Re_h > 10^4$ identified by Dimotakis[21] for a round jet.

Further insight into the Re dependence of a plane jet is sought by assembling data from previous investigations with closely matched initial conditions. A careful examination, however, reveals significant inconsistencies even for comparable Re_h and initial conditions. Figure 1 displays the centerline evolutions of locally normalized turbulence intensity,

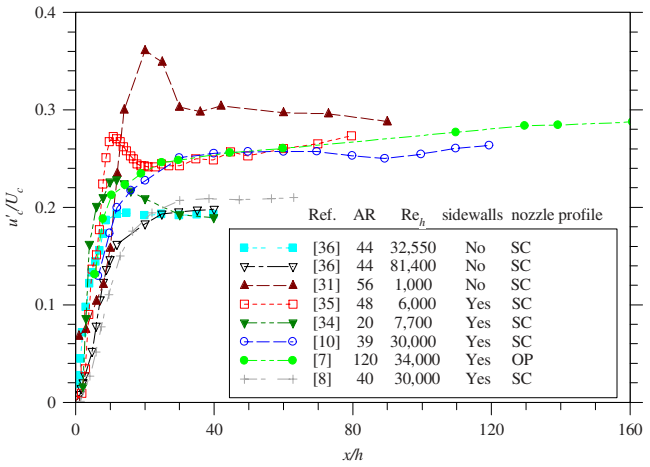

FIG. 1. (Color online) The streamwise evolution of the centerline turbulence intensity (u_c'/U_c) of previous investigations of a turbulent plane jet. The legend lists the nozzle AR, jet exit Reynolds number (Re_h), presence or absence of sidewalls in the *x-y* plane, and nozzle-exit geometric profiles (SC=smooth contraction; OP=orifice plate).

u_c'/U_c, reported in literature. Here, u_c' and U_c are the fluctuating and mean components of the centerline velocity. Among these data sets, the closest match is between those of Gutmark and Wygnanski[10] and Heskestad,[7] who measured a plane jet at similar Reynolds numbers but different AR and nozzle contraction profiles, so that they are not directly comparable. The two data sets agree closely within the midfield, i.e., $x/h \leq 60$, but exhibit some differences in the far field (for $x/h > 60$). Likewise, the results from smoothly contracting nozzles of Gutmark and Wygnanski[10] and Bradbury[8] for relatively high nozzle aspect ratios (AR=39 and 40) measured at identical Reynolds numbers ($Re_h = 30\,000$) differ significantly. These differences can probably be attributable to the use of a coflow by Bradbury[8] (for a coflow to jet velocity ratio of ≈16%). The work of Browne *et al.*[34] and Thomas and Goldschmidt[35] ($Re_h = 7700$ and 6000) reported measurements at different ARs (20 and 44), consistent with them exhibiting significant near-field differences. Thomas and Goldschmidt[35] and Namar and Ötügen[31] used similar values of AR and Re_h, except that the latter did not employ sidewalls. Likewise, the results of Hussain and Clark,[36] who studied plane jets for $Re_h = 32\,500$ and 81 400, show the lowest midfield turbulence intensity despite this value being similar to that of Browne *et al.*[34] of $Re_h \approx 7700$. Also importantly, their midfield turbulence intensity is significantly lower than those of Namar and Ötügen[31] who measured their jet at $Re_h = 7000$. In addition to the differences in initial conditions reported, other possible differences from laboratory to laboratory include surface finish and measurement uncertainties.

Thus the wide range of different operating/experimental conditions used in previous studies makes it impossible to isolate the effect of Reynolds number from those of other variables. It is also clear that systematic measurements of the influence of Re_h on a plane jet for $Re_h > 7500$ are presently not available. We seek to fill these gaps by systematically measuring (i) the flow field of a plane jet for Re_h varying

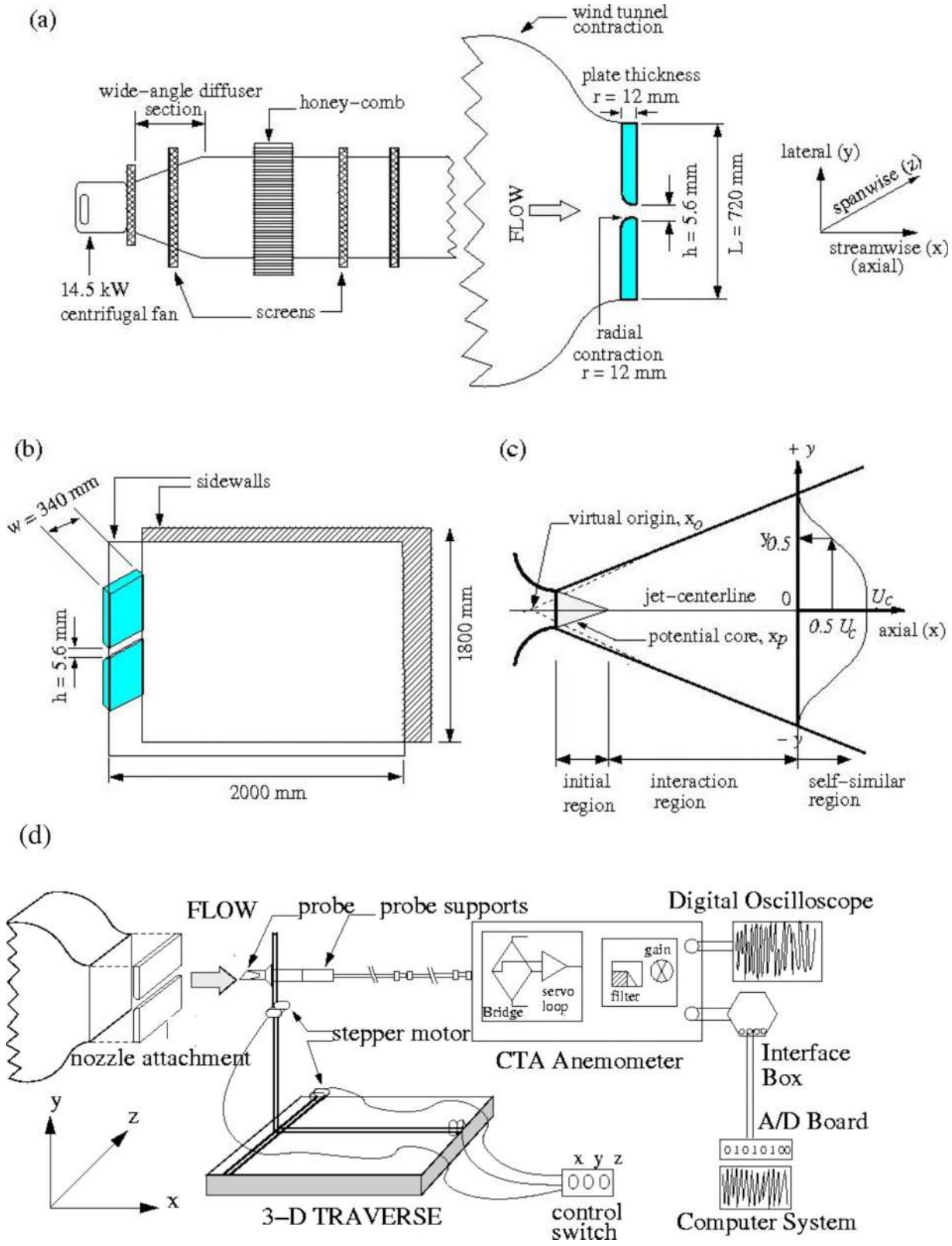

FIG. 2. (Color online) A schematic of the present experimental setup, showing (a) the wind tunnel details and nozzle attachment, (b) the side view showing nozzle parameters and sidewalls, (c) the jet development characteristics, and (d) the measurement apparatus. Note that diagrams drawn are not to scale.

between 1500 and 16 500, issuing from a radially contoured slot of AR=60 in detail, and (ii) the centerline velocity decay rate for Re_h varying between 4500 and 57 500, issuing from a radially contoured slot of AR=36 in the same flow facility. Our specific aim is to examine the dependence on Re_h of the mean velocity, the root mean square (rms), and high-order moments of the velocity fluctuation over a greater downstream distance ($0 \leq x/h \leq 160$) than has previously been reported. We also aim to relate this dependence to the underlying structures in the flow.

II. EXPERIMENT DETAILS

A schematic of the present plane jet facility is shown in Fig. 2, described in more detail by Deo.[15] Briefly, the facility consists of an open circuit wind tunnel made from wooden modules with polished inner surfaces. The tunnel is mounted to the roof and driven by a 14.5 kW aerofoil-type centrifugal fan mounted firmly to the floor to minimize vibrations. The tunnel employs a 25° wide-angle diffuser of 2100 mm in length, which expands into a settling chamber. Inside the diffuser are two screens with an open area ratio of ≈60% mounted at equal intervals of 600 mm. The screens assist in reducing the velocity defect in the turbulent boundary layer. The settling chamber is 1400 mm long and contains a honeycomb of drinking straws aligned horizontally with the main flow to reduce swirl. Following the honeycomb are three screens, each separated by 150 mm. There is followed by a 600 mm long settling chamber prior to the contraction to reduce turbulence intensity. To further enhance flow uniformity, the wind tunnel contraction has an area ratio of 6:1 and employs a smooth contraction profile based on a third order polynomial curve.

A plane nozzle with 12 mm radial contraction profile on its long sides [Fig. 2(a)] was mounted to the tunnel exit. The parallel sidewalls were flushed with the short sides of the slot and aligned along the x-y plane [Fig. 2(b)]. The sidewalls extended 2000 mm downstream and 1800 mm vertically and were secured tightly by bolts to the ceiling to avoid vibrations. The slot height (h), aligned with the lateral direction (y-plane) of the nozzle, was fixed at 5.60 mm. The slot span (w), aligned along the z-direction, was 340 mm to provide a large aspect ratio nozzle of AR$=w/h=60$. The fan pressure limited operation to $\mathrm{Re}_h \leq 16\,500$ for this nozzle. Hence, two other nozzles of AR=36 were designed, comprised of $(h,w)=(10\,360)$ and $(h,w)=(20\,720)$ mm, respectively, providing exit areas of 3600 and 14 400 mm^2, respectively. The latter allowed the maximum value of Re_h of 57 500 to be achieved. For all the cases, the exit radius of curvature is $r/h \geq 1.80$. This, according to our previous findings,[15,16] ensures that the exit mean velocity profile of the jet is approximately uniform.

The laboratory, acoustically isolated from external noise, is 18 000 mm long, 7000 mm wide, and 2500 mm high. The distance from the jet exit to the front wall of the room was $\approx 1400h$ and that between the jet and the ceiling/floor was $\approx 125h$. The plane jet was located horizontally at about the midpoint between the floor and ceiling. The ratio of the room height to the nozzle width was ≈446. Likewise, the ratio of the cross-sectional room area (in the same plane as the nozzle area) to the actual nozzle area was ≈10 000. Under these conditions, we used a similar model to that proposed by Hussein *et al.*[20] to assess the loss in streamwise momentum of the jet at different Re_h. It was found that, even at $x/h=160$ (the maximum downstream distance), the present jet sustains 99.2% and 99.5% of its initial streamwise momentum for $\mathrm{Re}_h=1500$ and 16 500, respectively. This confirms that the present jet closely resembles a truly unconfined jet.

Re_h was controlled by adjusting the speed of the wind tunnel fan to provide a momentum-averaged mean discharge velocity U_b varying between 3.98 and 44.20 m s^{-1} and achieve $\mathrm{Re}_h=1500-16\,500$ for AR=60. For AR=36, $w \times h=3600$, jets with U_b between 3 and 38.5 m s^{-1} were measured, corresponding to $2000 \leq \mathrm{Re}_h \leq 26\,000$, and for AR=36, $w \times h=14\,400$, jets with $3.37 \times U_b \times 42.4$ m s^{-1} were measured, corresponding to $4500 \leq \mathrm{Re}_h \leq 57\,500$.

The measurements were performed over the flow region $0 \leq x/h \leq 160$ using a single hot-wire anemometer, under isothermal conditions of ambient temperature 20.0 °C ± 0.1 °C. A custom-built (tungsten) hot-wire sensor (diameter $d_w=5$ μm and length $l_w=0.8$ mm) was used, with the overheat ratio of 1.5. The square wave test revealed that the maximum response frequency of the wire was 15 kHz. To avoid aerodynamic interference of the prongs on the hot wire, the present probe was carefully mounted, with prongs parallel to the plane jet. This alignment is appropriate for measurement of the streamwise component of the flow velocity, although it is not possible to eliminate directional ambiguity completely. The single wire probe, if used with caution, encounters reduced errors when compared with dual or triple wires because the adjacent probe can probably influence the measured velocity for the later cases. On the centerline of a plane jet, the cross-steam velocity is very small (must be zero on average) so that the uncertainty due to directional ambiguity is insignificant.

Calibrations of the hot-wire were conducted using a standard Pitot static tube, connected to hand-held digital manometer, located side by side with the hot-wire probe at jet exit plane (where $\langle u^2 \rangle^{1/2}/U_c \approx 0.5\%$) prior to and after each set of measurements. Data points were converted from voltages to velocities using a fourth order polynomial curve. Both calibration functions were checked for discrepancies, and the experiment was repeated if the velocity drift exceeded 0.5%. The average accuracy of each calibration function was found to be within ±0.2%. Velocity signals obtained were low pass filtered with an identical cutoff frequency of $f_c=9.2$ kHz at all measurement locations to eliminate excessively high-frequency noise. Then the voltage signals were offset to within 0–3 V as a precautionary measure to avoid signal clipping[37] and amplified appropriately through the circuits. They were digitized on a personal computer at $f_s=18.4$ kHz via a 16 channel, 12 bit PC-30F A/D converter with signal input range of 0–5 V. The sampling period was approximately 22 s, during which about 4×10^5 data points were collected at each measured location.

Using the inaccuracies in calibration and observed scatter in present measurements, the uncertainties are estimated to have a mean error of ±4% at the outer edge of the jet and ±0.8% on the centerline. The errors in the centerline mean velocity, rms velocity, the skewness, and the flatness were found to be approximately ±0.8%, ±1.8%, ±2%, and ±1.5%, respectively. The errors in the momentum integral quantities and jet virtual origins are estimated to be ±3%.

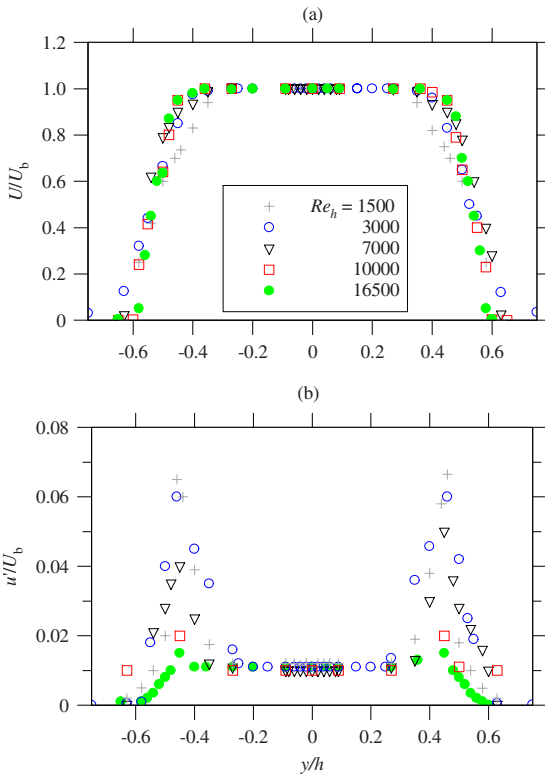

FIG. 3. (Color online) Lateral profiles of (a) the normalized mean velocity and (b) the turbulence intensity measured $x/h=0.5$ for plane jets with different Re_h values.

III. RESULTS AND DISCUSSION

A. Characterization of the exit conditions

The exit conditions were characterized by measuring the velocity profiles in each plane jet at $x/h=0.5$ along the lateral (y) direction over the range $-0.70 \le y/h \le 0.70$ [Figs. 3(a) and 3(b)]. Dependence of the exit flow on Re_h is evident. All cases produce an approximately top-hat mean exit velocity profile. However, the extent of uniformity in the profiles differs significantly. As Re_h is increased from 1500 to 16 500, the exit velocity profiles become flatter, and the horizontal region of uniformity widens. A consistent trend in the initial turbulence intensity u' is evident from Fig. 3(b). The peak value of u'/U_b decreases with Re_h while the centerline value remains almost constant at about 1.0%. Also, the mean exit velocity profiles for $\mathrm{Re}_h=10\,000$ and 16 500 are nearly indistinguishable, although some differences are evident in the peak values of u'/U_b within the shear layers.

The initial boundary layer characteristics may be estimated from the measurements at $x/h=0.50$ (the profiles closest to the nozzle). The displacement thickness $(\delta_{0.5})$, the momentum thickness $(\theta_{0.5})$, and the shape factor $(H_{0.5}=\delta_{0.5}/\theta_{0.5})$ were calculated approximately from these mean velocity profiles and the momentum integral equations, viz.,

$$\delta_{0.5} = \int_0^\infty (1 - U/U_b)_{x=0.5h} dy \tag{1}$$

and

TABLE I. A summary of the normalized boundary layer characteristics estimated from mean velocity profiles at $x/h=0.5$ for different Re_h.

Re_h	Displacement thickness $\delta_{0.5}$	Momentum thickness $\theta_{0.5}$	Shape factor $H_{0.5}$
1500	$0.133h$	$0.068h$	1.95
3000	$0.116h$	$0.056h$	2.09
7000	$0.109h$	$0.045h$	2.43
10 000	$0.098h$	$0.040h$	2.45
16 500	$0.097h$	$0.039h$	2.49

$$\theta_{0.5} = \int_0^\infty (U/U_{o,c})(1 - U/U_b)_{x=0.5h} dy. \tag{2}$$

Table I presents the averages of the above parameters calculated independently on each side of the profile using "best-fit" spline curves and numerically integrating Eqs. (1) and (2). Although the measurement resolution is somewhat coarse, clear trends are evident. As Re_h is increased from 1500 to 16 500, both $\delta_{0.5}$ and $\theta_{0.5}$ decrease from approximately $0.133h$ to $0.097h$ and $0.068h$ to $0.039h$, respectively. This agrees qualitatively with other measurements for a round jet[18,38] and also that for a high-AR rectangular jet.[31]

B. The mean velocity field

Figure 4 presents the axial variation of centerline mean velocity (U_c) normalized by the bulk mean velocity at the exit (U_b) for $1500 \le \mathrm{Re}_h \le 16\,500$ in log-log form. First we consider the near field. It is evident that the length of the potential core, x_p, in which U_c is constant, exhibits a Re_h dependence. This can be seen more clearly in Fig. 5, which presents the dependence of x_p, defined to be the axial location at which $U_c(x) \approx 0.98 U_{o,c}$ on Re_h. This demonstrates that x_p decreases asymptotically with Re_h, consistent with previous results for a round jet[39] and for a high-AR rectangular jet.[31] This implies that increasing Re_h will increase jet entrainment in the near field. The comparison in Fig. 6 of the lateral profiles of U_c at $x/h=5$ for the different Re_h lends

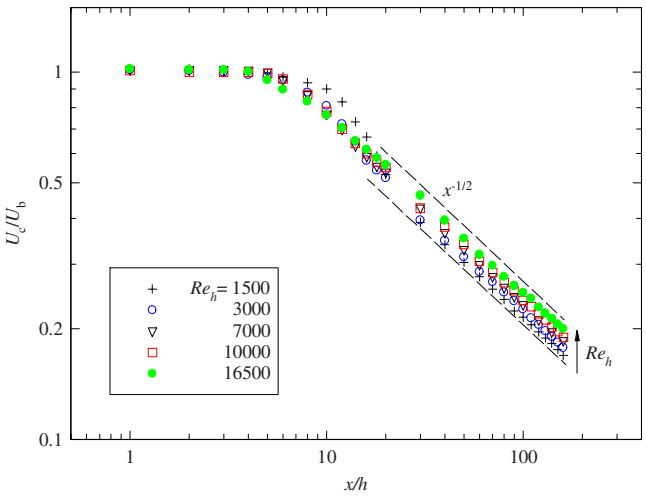

FIG. 4. (Color online) The evolution of mean centerline velocity (U_c/U_b) for a plane jet with different Re_h values.

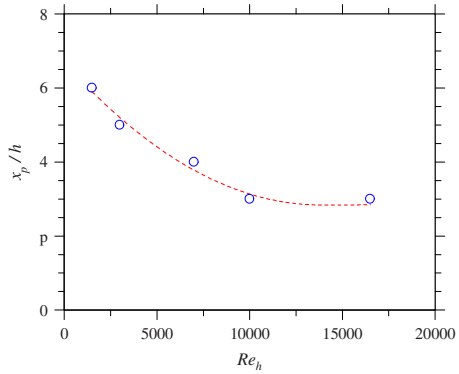

FIG. 5. (Color online) The dependence of the jet's potential core lengths (x_p) on jet exit Reynolds number (Re_h).

support to this deduction. Evidently the jet spread in the near field increases with Re_h. From Table I, this near-field increase is associated with a decrease in the exit boundary layer thickness.

Next we return to Fig. 4 to assess the influence of Re_h on the far field using the well-known similarity relationship for a plane jet,

$$(U_b/U_c)^2 = K_u(x/h + x_{01}/h)$$
$$\text{or} \quad U_c/U_b = [K_u(x/h + x_{01}/h)]^{-1/2}. \tag{3}$$

This becomes valid from the transition region following the potential core. Here, the constant K_u is the slope of $(U_b/U_c)^2$, which is a measure of the decay rate of U_c, and x_{01} is the x-location of the virtual origin of $(U_b/U_c)^2$. Although the present data for AR=60 appear to converge asymptotically, the asymptotic value of convergence cannot be determined from these data because it exceeds 16 500. However, it is evident from the jets from the other two nozzles, w/h=360/10 and 720/20, that K_u converges asymptotically for each jet at $\mathrm{Re}_h \approx 25\,000$ (Fig. 7). However, the jets from the different nozzles do not converge onto the same line due to their different inflow boundary conditions. Figure 7 also reveals a consistent trend that the decay rate of plane jet

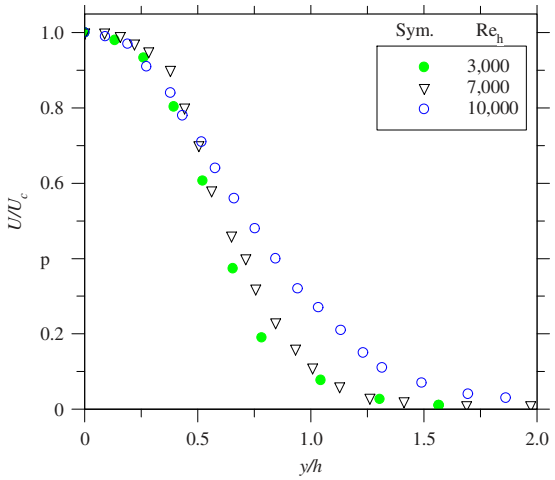

FIG. 6. (Color online) The dependence of lateral profiles of U/U_c on Re_h measured at x/h=3.

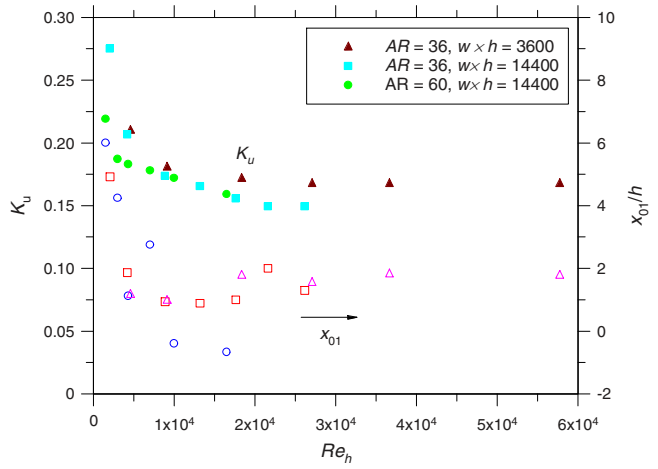

FIG. 7. (Color online) Dependence on Re_h of K_u (filled symbols) and x_{01}/h (open symbols) for AR=60 (r/h=2.14) and AR=36 (r/h=1.80) for two values of w and h.

decreases as Re_h is increased. The dependence of x_{01} on Re_h follows a similar trend to that of K_u, although with greater scatter (as is typical for this measurement). Once again, the data do not collapse onto a single curve due to the differences in initial conditions.

Figure 8 presents the lateral profiles of U/U_c at selected downstream locations for the AR=60 jet. Here, the y-coordinate is normalized using the velocity half-width $y_{0.5}$, determined from the location at which $U(x,y)=\frac{1}{2}U_c(x)$. As

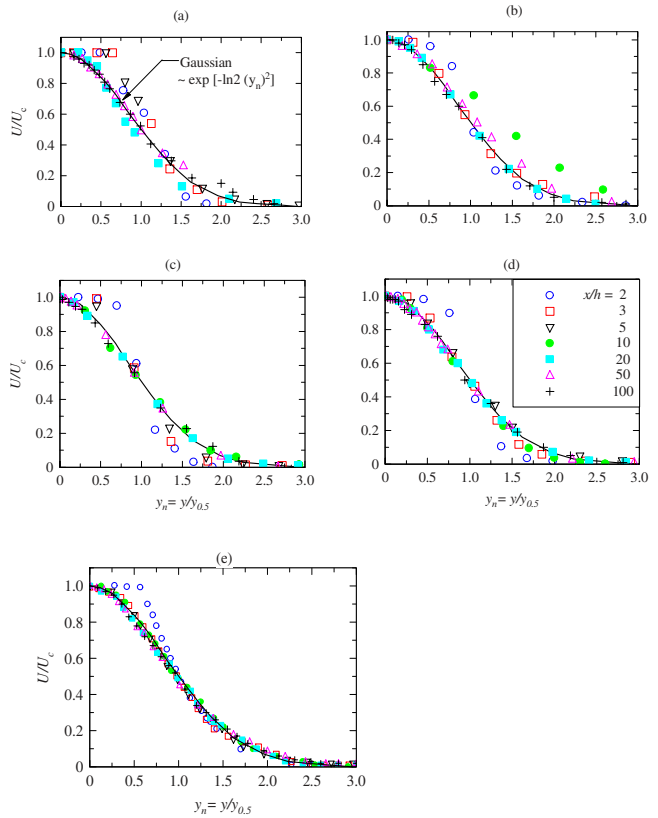

FIG. 8. (Color online) Lateral distributions of U/U_c for AR=60: (a) Re_h =1500, (b) Re_h=3000, (c) Re_h=7000, (d) Re_h=10 000, and (e) Re_h =16 500.

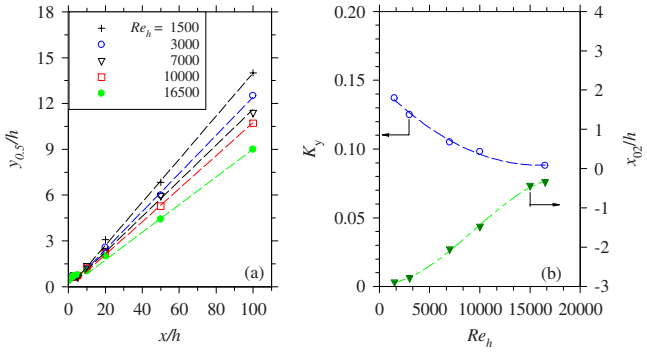

FIG. 9. (Color online) (a) Streamwise evolution of $y_{0.5}/h$ for Re_h = 1500–16 500. (b) Dependence of the spreading rate (K_y) and virtual origin (x_{02}/h) on Re_h.

expected, the velocity profiles become self-similar at a shorter downstream distance when the Reynolds number is higher. For instance, self-similarity is attained at $x/h > 5$ for $\mathrm{Re}_h = 16\,500$ and at $x/h > 20$ for $\mathrm{Re}_h = 1500$. The self-similar velocity profiles conform closely to the Gaussian distribution $U_n = e^{-\ln 2 (y_n)^2}$, where $U_n = U/U_c$ and $y_n = y/y_{0.5}$.

The influence of Re_h on the mean spreading rate of the AR=60 jet is assessed from the half-width $y_{0.5}$. Figure 9(a) shows that the half-widths vary linearly with x for $x/h > 10$ for all the present Reynolds numbers. This linear variation can be represented by

$$y_{0.5}/h = K_y(x/h + x_{02}/h), \tag{4}$$

where the slope K_y is a nominal measure of the jet spreading rate and x_{02} is the virtual origin of jet spread. Figure 9(b) demonstrates that as Re_h increases from 1500 to 16 500, K_y decreases asymptotically from about 0.14 to 0.09, while x_{02} increases from about −3 to 0. This trend of K_y is consistent with that of K_u (Fig. 5). Taking them together, we conclude that an increase in Re_h leads to the reduced entrainment of the jet in the far field. This is opposite to the near-field trend (see Fig. 6), as will be discussed below.

Next we consider the local Reynolds number defined by $\mathrm{Re}_{y0.5} \equiv 2U_c(x)y_{0.5}(x)/\nu$. Figure 10(a) shows the streamwise variation of $\mathrm{Re}_{y0.5}$ for different values of Re_h. It is clear that

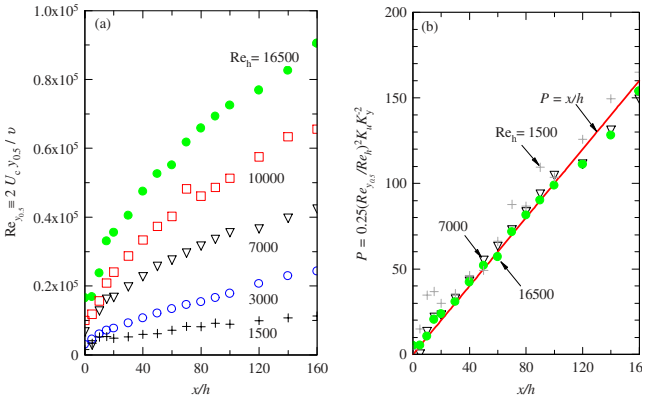

FIG. 10. (Color online) Streamwise evolution of (a) the local Reynolds number ($\mathrm{Re}_{y0.5}$) for Re_h = 1500–16 500 and (b) the data scaled according to Eq. (5).

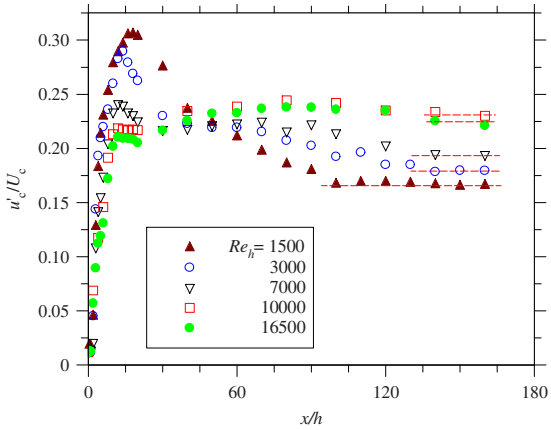

FIG. 11. (Color online) Streamwise evolution of u'/U_c for Re_h = 1500–16 500.

$\mathrm{Re}_{y0.5}$ increases with axial distance for each value of Re_h. This occurs because the far-field decay rate of U_c is lower than the growth rate of $y_{0.5}$, as is evident from Eqs. (3) and (4). Combining Eqs. (3) and (4), the local Reynolds number in the self-similar region should vary as

$$\mathrm{Re}_{y_{0.5}} = 2\ \mathrm{Re}_h K_y K_u^{-1/2}[(x - x_o)/h]^{1/2}. \tag{5}$$

To check relation (5), we plot in Fig. 10(b) the results of $P = 0.25(\mathrm{Re}_{y_{0.5}}/\mathrm{Re}_h)^2 K_u K_y^{-2}$ versus x/h for Re_h=1500, 7000, and 16 500. Good collapse of the data is evident, within experimental uncertainties. That is, Eq. (5) is approximately valid with $x_o \approx 0$. Note that Eq. (5) appears to work even in the very near field where Eqs. (3) and (4) are not valid. We can thus conclude that $\mathrm{Re}_{y0.5}$ increases with the downstream evolution of a plane jet and must eventually become very high no matter how low its initial value is. This is in contrast to the case for the axisymmetric jet or plane wake where the local Reynolds number remains constant in the far field. Also of interest, the opposite occurs in the axisymmetric wake, where the local Reynolds number decreases with increasing x.[40] Note that this increase in $\mathrm{Re}_{y0.5}$ with x/h does not mean that plane jets will eventually converge to the same asymptotic state with axial distance since the dependence of far-field state on Re_h has already been described above. It is also interesting to note that at x/h=160, $\mathrm{Re}_{y0.5}$ reaches the order of 10^5 for Re_h=16 500 but only of 10^4 for Re_h=1500.

C. The fluctuating velocity field

Figure 11 presents the centerline evolution of the turbulence intensity ($u_c^* = u_c'/U_c$) for different values of Re_h. Evidently, as x is increased, u_c^* grows rapidly from the exit value of about 1% to the local maximum ($u_{c,\max}^*$), then decreases to gradually converge to an asymptotic value ($u_{c,\infty}^*$) in the far field. However, the magnitudes and axial locations ($x_{\max}^*, x_\infty^*$) of both $u_{c,\max}^*$ and $u_{c,\infty}^*$ are dependent on Re_h. Several observations can be made. First, as Re_h is increased from 1500 to 16 500, both $u_{c,\max}^*$ and $x_{\max}^*$ decrease together from 0.31 to 0.22 and from 18 to 12, respectively (see Fig. 12). However, $u_{c,\max}^*$ and $u_{c,\infty}^*$ exhibit opposite dependence on Re_h, so that the lowest Re_h exhibits the highest $u_{c,\max}^*$ and the lowest $u_{c,\infty}^*$. This results in the near-field peak being overwhelmingly

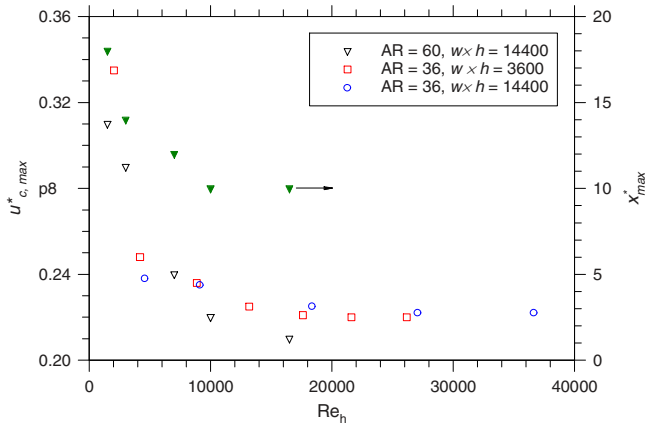

FIG. 12. (Color online) Dependence on Re_h of $u'_{c,max}$ and its axial location (x^*_{max}).

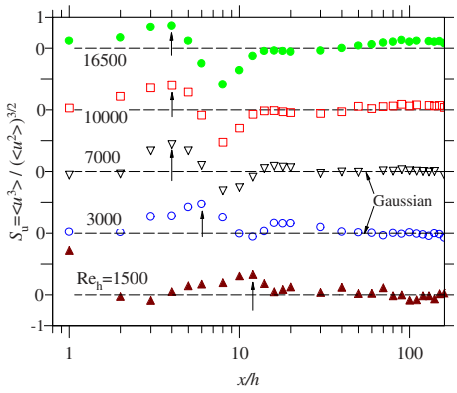

FIG. 14. (Color online) Streamwise evolutions of S_u for Re_h = 1500–16 500. Symbols are identical to Fig. 11.

dominant for low Re_h, while for high Re_h the near-field peak is almost nonexistent and the far-field "peak" is dominant. Finally, there is general consistency in the asymptotic values of the present data and those presented earlier (Fig. 7), with both $u^*_{c,\infty}$ and x^*_∞ becoming independent of Re_h at about $Re_h \geq 25\,000$ (Fig. 13). However, there is some scatter, with $u^*_{c,\infty}$ reaching the asymptotic state at $Re_h \approx 40\,000$.

The increase of present $u^*_{c,\infty}$ with Re_h found here stands in contrast to the observation of Namar and Ötügen[31] that an increase in Re_h led to a decrease in $u^*_{c,\infty}$. The probable explanation for this apparent discrepancy is that their study did not employ sidewalls, so that their jet exhibits a different behavior, such as axis switching. Our previous investigation[17] has shown that although a high-AR-rectangular nozzle without sidewalls produces a statistically two-dimensional plane-jet-like region, the overall magnitudes of flow statistics are significantly different from those in the same rectangular nozzle with sidewalls.

Figures 14 and 15 display the centerline evolutions of the skewness $S_u[\equiv\langle u^3\rangle/\langle u^2\rangle^{3/2}]$ and flatness $F_u[\equiv\langle u^4\rangle/\langle u^2\rangle^2]$ at the different values of Re_h. These provide measures of the symmetry and flatness, respectively, of the probability density function (PDF) of u. Both S_u and F_u were estimated from a large data sample (≈400 000 data points) to achieve the convergence of the PDF. During measurements a voltage offset was applied to the analog-to-digital range of the A/D board to ensure that neither factors were truncated due to clipping of the tails of the PDFs, as can occur for a finite input range of the sampling board. Also note that a higher scattering of the far-field data of S_u for Re_h=1500 is due to its relatively low velocity (<1 m/s for $x/h > 70$) and thus a

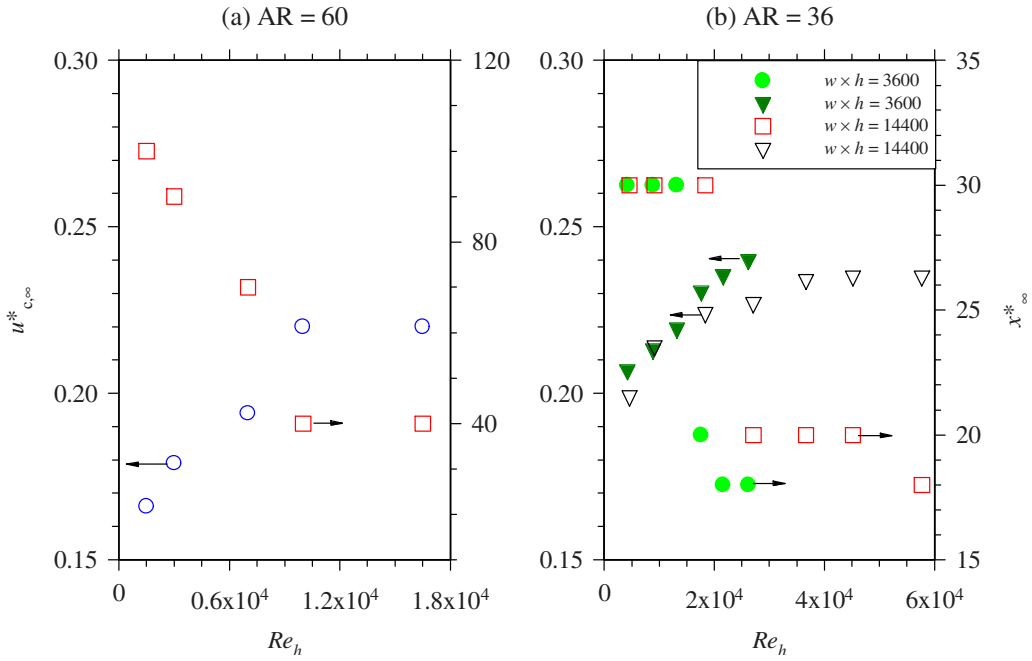

FIG. 13. (Color online) Re_h dependence of the asymptotic value of $u^*_{c,\infty}$ and the axial location (x^*_∞) at which the turbulence intensity asymptotes for the cases (a) AR=60 and (b) AR=36. Note that for AR=36, two nozzles of different exit areas ($w \times h$=3600 and 14 400) were tested.

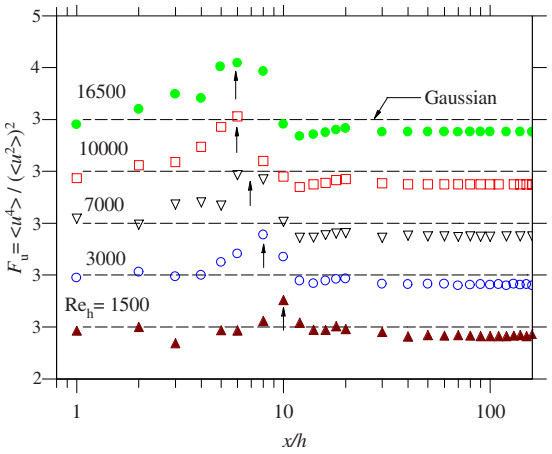

FIG. 15. (Color online) Streamwise evolutions of F_u for Re_h =1500–16 500. Symbols are identical to Fig. 11.

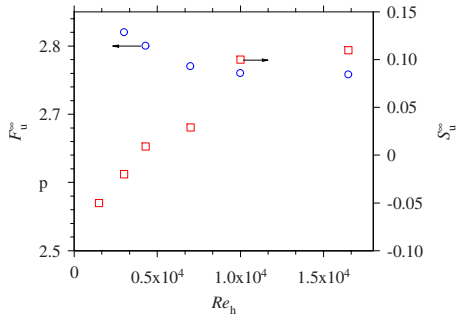

FIG. 16. (Color online) Dependence of the asymptotic value of S_u^∞ and F_u^∞ on Re_h.

high uncertainty for this case; the estimation of F_u is more accurate than that of S_u since $F_u \gg |S_u|$, and generally S_u is small.

Both factors vary dramatically in the near-field region ($x/h \leq 30$), presumably owing to the dominance of large-scale coherent motions in the near-field region. Moving downstream from the exit, both S_u and F_u increase from nearly Gaussian values of (0, 3) to highly non-Gaussian local maxima in the vicinity of the end of the potential core. This local maximum in S_u occurs between $4 \leq x/h \leq 12$ (indicated by arrows on the plot) while that for F_u occurs around $5 \leq x/h \leq 10$ (Fig. 15). They then decrease to a local minimum before increasing gradually to their asymptotic values by $30 \leq x/h \leq 40$. In general, as Re_h increases, the near-field maxima increase, and their x-locations translate upstream. The latter is consistent with the shortening of x_p (Fig. 5), increased near-field entrainment (Fig. 6), and a reduction in $x_{\max}$ (Fig. 12). More coherent motions in the shear layers are evidenced by less random fluctuations, i.e., by more departure of the PDF from the Gaussian distribution and of S_u and F_u from the values of 0 and 3, respectively. In addition, Figs. 14 and 15 show that S_u and F_u approach their respective asymptotic values, $S_u^{c,\infty}$ and $F_u^{c,\infty}$, at $x/h \geq 40$ nearly for all values of Re_h. However, both $S_u^{c,\infty}$ and $F_u^{c,\infty}$ exhibit a consistent, albeit weak dependence on Re_h. Overall, as Re_h is increased, $S_u^{c,\infty}$ decreases and $F_u^{c,\infty}$ increases (Fig. 16).

Next we assess the effect of Re_h on the small-scale turbulence by examining the centerline dissipation rate (ε) of the turbulent kinetic energy at different values of Re_h. For high-Re flows, it is usually considered that the dissipation of turbulent kinetic energy by the smallest-scale structures is equal to the supply rate of the turbulence energy from the large-scale structures, which is of order U_o^3/L_o, where U_o and L_o are the local characteristic velocity and length scales (see, e.g., Ref. 41). Based on this argument, we obtain the centerline dissipation $\varepsilon \sim U_c^3/y_{0.5}$ by taking $U_o = U_c$ and $L_o = y_{0.5}$ for a plane jet. It follows from Eqs. (3) and (4) that self-preservation of the flow further requires

$$\varepsilon(hU_b^{-3}) = C_\varepsilon (x/h)^{-5/2}, \tag{6}$$

and thus the smallest scale or Kolmogorov scale, defined by $\eta \equiv (\nu^3/\varepsilon)^{1/4}$, to follow

$$\eta/h = C_\varepsilon^{-1/4}\, \mathrm{Re}_h^{-3/4} (x/h)^{5/8}, \tag{7}$$

where C_ε is determined by experiments. It is evident from Eq. (7) that the smallest scale η decreases with increasing Re_h. Here we check the above relations and especially the effect of Re_h on C_ε. To estimate ε from the time derivative of u_c, as in literature, both the isotropic assumption $\varepsilon = 15\nu\langle(\partial u_c/\partial x)^2\rangle$ and Taylor's hypothesis $\partial u_c/\partial x = U_c^{-1}\partial u_c/\partial t$ are invoked. Figure 16 illustrates the present results, together with that of Antonia *et al.*[42] for Re_h=22 000. As is well known, accurate dissipation measurements require full spatial and temporal resolutions of the smallest-scale fluctuation in velocity.[43,44] Estimation of the Kolmogorov frequency f_K (corresponding to the smallest-scale fluctuation) based on the iterative scheme developed by Mi *et al.*[45] suggests that the present measurements (low-pass cutoff at 9.2 kHz) can resolve the smallest-scale fluctuations of u at $x/h \geq 0$, 20, and 70 for Re_h=1500, 3000, and 7000, respectively, but cannot do so for Re_h=10 000 and 16 500 within the measured range of x/h. Accordingly the present data of ε and η shown in Fig. 17 are only for Re_h=1500, 3000, and 7000.

Figure 17 indicates that both relations (6) and (7) are approximately valid in the far field of a plane jet at least for $\mathrm{Re}_h \geq 1500$. Interestingly this validity appears to occur just downstream from x/h=20 for all the Reynolds numbers including the lowest Re_h=1500. This is beyond the conventional consideration since the distance of $20h$ is shorter than those required for achieving the asymptotic values of u'/U_c or of the skewness and flatness factors (see Figs. 14 and 15). Similar observations can be also made from Figs. 2–4 and 6 of Ref. 42 for both plane and circular jets. It is well known that the dissipation rate reflects the statistical behavior of the smallest-scale turbulence while other properties shown above are for the large-scale turbulence. This seems to suggest that the asymptotic state is more easily achieved by small-scale turbulence than by large-scale turbulence. Clearly further investigations are needed to address this issue more comprehensively.

Figure 17 also shows that as Re_h is increased, both C_ε and η decrease. However, C_ε depends not only on Re_h but

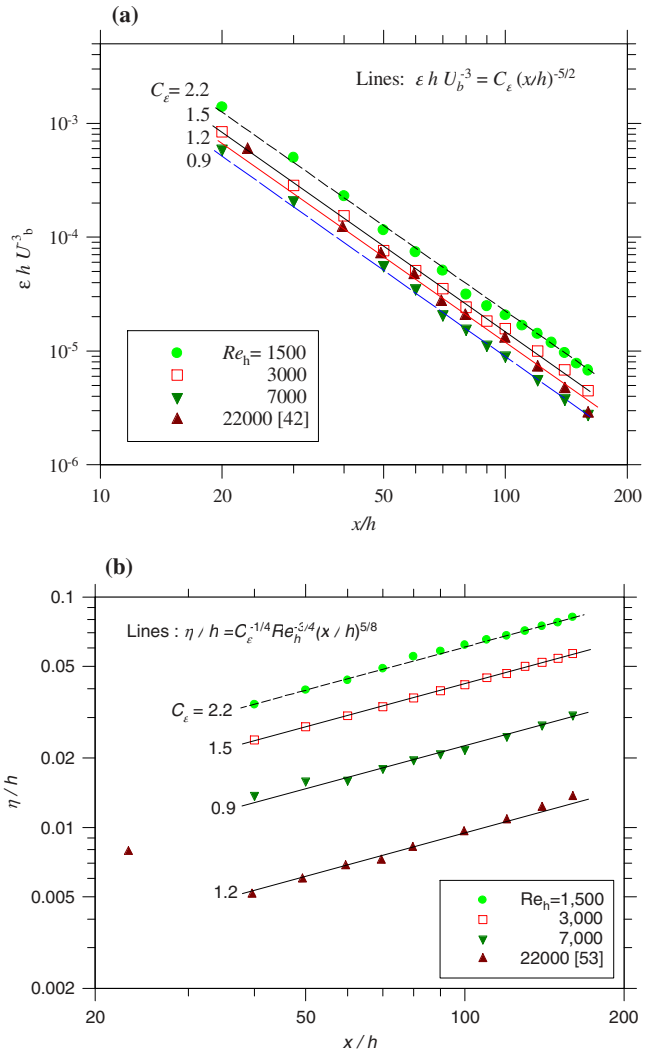

FIG. 17. (Color online) Streamwise evolution of (a) turbulent kinetic energy dissipation ($\varepsilon h U_b^{-3}$) and (b) Kolmogorov scales (η/h) for the present cases Re_h=1500, 3000, and 7000, as well as those of Ref. 42 (Re_h=22 000).

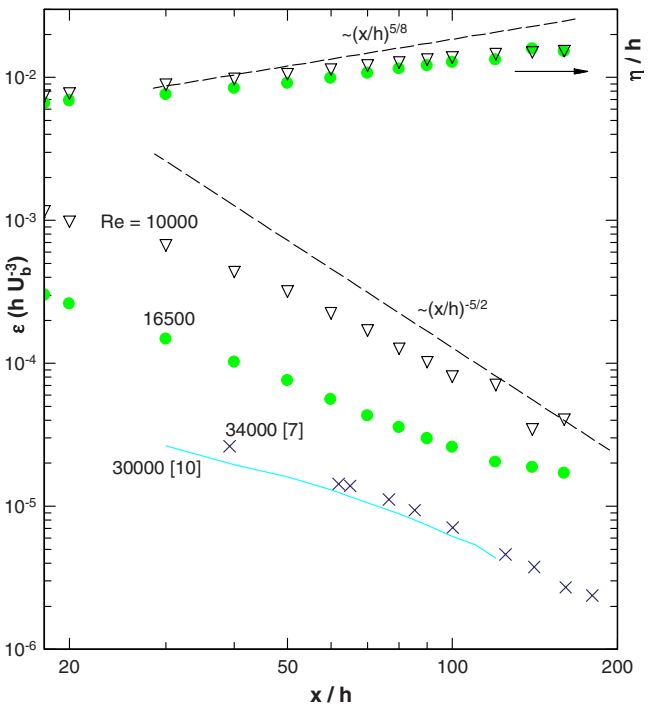

FIG. 18. (Color online) Streamwise evolutions of $\varepsilon h U_b^{-3}$ and η/h for the present cases of Re_h=10 000 and 16 500 and for Ref. 10 (Re_h=30 000) and Ref. 7 (Re_h=34 000).

also on other initial and/or boundary conditions, so that its value for Re_h=22 000 estimated from the measurements of Antonia *et al.*[42] is higher than that deduced from the present trend. Note that the impact of C_ε on the Re_h dependence of the dissipation rate is relatively small. This can be seen in the alternative form of Eq. (6), i.e.,

$$\varepsilon = C_\varepsilon \, Re_h^3 \nu^3 h^{-4} (x/h)^{-5/2}. \tag{8}$$

That is, ε increases cubically (i.e., at a rate much higher than that of decrease of C_ε) as Re_h (or U_b) increases. For example, when Re_h is increased from 1500 to 7000, ε rises by approximately 4100% while C_ε reduces by only 144%. The dependence of η on x/h is shown in Fig. 17(b) for constant values of Re_h. The good agreement with Eq. (8) confirms that the data are well resolved for these Re_h.

Figure 18 assesses those data, both from the present measurement and past investigations that do not adequately resolve the smallest scales of turbulence. This is done by scaling the data according to Eq. (6). The departure of our data from the scaling by $(x/h)^{-5/2}$ is evident for Re_h =10 000 and 16 500, as discussed above, consistent with the strong dependence of η on Re_h [Fig. 17(b)]. Figure 18 also shows that the results of ε reported in Refs. 7 and 10 for Re_h=36 000 and 30 000, respectively, also do not resolve the smallest scales of turbulence. Both of these studies had a too poor frequency response for adequate resolution of ε.

IV. FURTHER DISCUSSION

It is evident that the statistical properties of the streamwise velocity field of plane jets depend strongly on Re_h up to the asymptotic value, both in the near field and the far field, with nonidentical states of self-similarity. To provide some explanations, we examine the Re dependence of the power spectra of u and use these to assess the underlying coherent structures at different values of Re_h.

A. Spectral results of different Reynolds numbers

The existence of large-scale coherent structures in the near field of a turbulent plane jet has been well demonstrated by previous studies.[6,46–49] These near-field structures can occur symmetrically or antisymmetrically with respect to the jet centerline, termed the "symmetric mode" and "antisymmetric mode," respectively. As revealed by Sato,[6] Rockwell and Niccolls,[48] and Thomas and Goldschmidt,[49] the symmetric mode occurs in a jet issuing from a smooth contraction nozzle, whose exit mean velocity is nearly uniform or in a "top-hat" shaped profile. The long channel or pipe nozzle produces a power-law profile of the exit mean velocity and leads to the initial dominance of antisymmetric modes for the jet.[50] The presence of these structures can be detected in

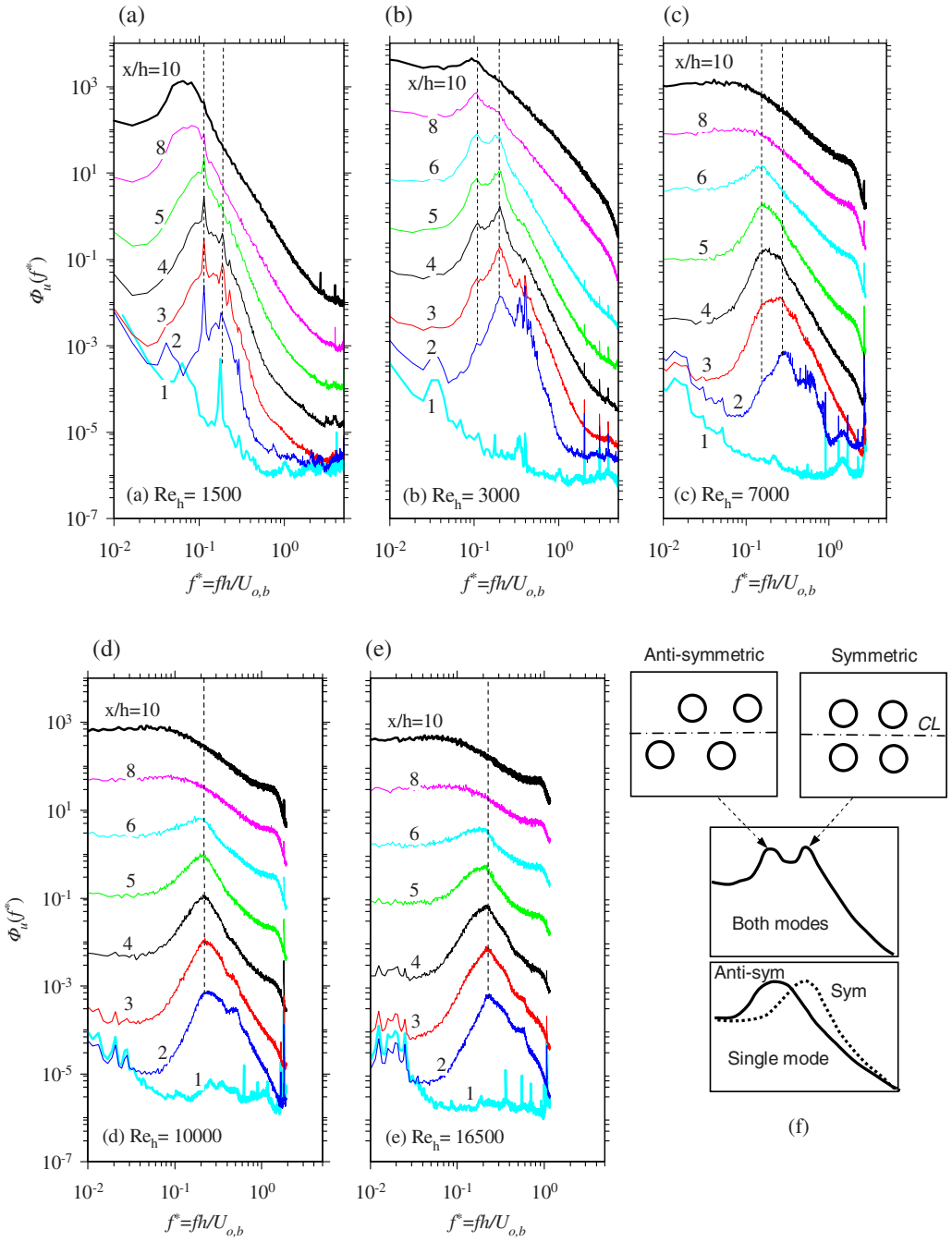

FIG. 19. (Color online) Centerline spectra (Φ_u) of the velocity fluctuation (u) measured between $x/h=1$ and $x/h=10$ for (a) Re$_h$=1500, (b) Re$_h$=3000, (c), Re$_h$=7000, (d) Re$_h$=10 000, (e) Re$_h$=16 500, and (f) a schematic of Φ_u, showing the symmetric and antisymmetric modes based on previous observation of Ref. 6. Note that CL denotes the centerline.

power spectra of the fluctuating velocity (Φ_u). Figure 19 presents the centerline evolution of Φ_u from $x/h=1$ to $x/h=10$, where Φ_u is defined in $\langle u^2\rangle=\int_0^\infty \Phi_u df$ and the normalized frequency is $f^*=fh/U_b$. Figure 19(f) illustrates schematically how the peak values of Φ_u can be used to assess whether the symmetric and/or antisymmetric modes are dominant. This is based on previous observations[6] that the passage frequency of the primary vortices detected by the probe on the centerline should be lower for the antisymmetric mode than for the symmetric mode. In this context, it is important to note that the values of f^* obtained on and off the centerline are identical, so that we present only the centerline data here.

Figure 19 demonstrates that, very close to the nozzle at $x/h\leq 1$, no fundamental (or dominant) peaks in Φ_u can be identified in the range $0.1\leq f^*\leq 0.3$, indicating that this is upstream from the location where primary vortices form. Further downstream at $x/h\geq 2$, such peaks are present, demonstrating that these vortices are present within the shear layers and are thus detected by the probe on the centerline.

However, distinct characteristics of Φ_u are evident for different Reynolds numbers. Evidently, when $\mathrm{Re}_h \leq 7000$, Φ_u is bimodal over the range $0.1 \leq f^* \leq 0.3$, whereas for $\mathrm{Re}_h \leq 10\,000$, it is broadly unimodal at $f^* \approx 0.22$. It is hence deduced that both modes occur for $\mathrm{Re}_h \leq 7000$ and that their relative importance varies with Re_h. For $\mathrm{Re}_h = 1500$, the antisymmetric mode appears to dominate the near field from $x/h=1$ to 5. Further downstream at $x/h=8$ and 10, the pairing of primary vortices occurs, and the peak in Φ_u shifts to lower frequencies [Fig. 19(a)]. That the first shift in f^* for the $\mathrm{Re}_h \leq 7500$ is due to a transition between the mode type rather than vortex pairing can be deduced from the finding that this transition does not occur for $\mathrm{Re}_h \geq 10\,000$. Further downstream, the primary vortices break down and less coherent structures develop. It is deduced below that these far-field structures take the antisymmetric mode.

For $\mathrm{Re}_h < 10\,000$, the near-field, streamwise evolution of Φ_u suggests that the symmetric mode becomes increasingly important over the range $x/h \leq 8$ as Re_h is increased. That is, although both modes of the primary vortical structures coexist in the near field, the symmetric mode becomes overwhelmingly prevailing as Re_h is increased. This differs from the finding of Sato.[6] He concluded that the symmetric and antisymmetric modes occur, respectively, in plane jets with uniform profiles (from a smooth contraction) and parabolic profiles (from a long channel) of the exit mean velocity. One reason for this apparent discrepancy may be that Sato[6] did not use sidewalls for his plane jets. It is also possible that his smooth contraction produced more uniform exit velocity profiles than the present nozzles.

The jets of $\mathrm{Re}_h = 10\,000$ and 16 500 have highly uniform exit velocity profiles (see Fig. 3). Under these circumstances the primary vortices in the two mixing layers are expected to solely exhibit the symmetric mode. This is indeed the case, as reflected by a significant single broad peak in Φ_u at $f^* \approx 0.22$ for all cases other than a weak secondary peak at $x/h=2$. Moreover it is important to note that the distributions of Φ_u are quite similar at all the x locations in the two jets, suggesting the statistical similarity of their near-field underlying structures. It also demonstrates that no vortex pairing occurs for these jets.

Figure 20 demonstrates the Re dependence of the Strouhal numbers for the two modes ($\mathrm{St}_{\mathrm{sym}}, \mathrm{St}_{\mathrm{ant}}$). The values of $\mathrm{St}_{\mathrm{sym}}$ and $\mathrm{St}_{\mathrm{ant}}$ are those of f^* corresponding to obvious peaks of Φ_u at $x/h=2-6$, as indicated in Fig. 19 by dashed lines. (Note again that the results of $\mathrm{St}_{\mathrm{sym}}$ and $\mathrm{St}_{\mathrm{ant}}$ obtained on and off the centerline are identical so that we present here the centerline data only.) Figure 20 also shows the results of Sato[6] for comparison. It appears that an increase in the Reynolds number from $\mathrm{Re}_h = 1500$ to $\mathrm{Re}_h = 7000$ causes both $\mathrm{St}_{\mathrm{sym}}$ and $\mathrm{St}_{\mathrm{ant}}$ to increase slightly, implying a weak dependence on Re_h of the vortex shedding. This contrasts the previous results of Sato,[6] who reported that $\mathrm{St}_{\mathrm{sym}}=0.23$ and $\mathrm{St}_{\mathrm{ant}}=0.14$ over the range $\mathrm{Re}_h = 1500-8000$, and Namar and Ötügen,[31] who reported that $\mathrm{St}_{\mathrm{sym}}=0.273$ for $\mathrm{Re}_h = 1000-6000$. Again we note that it is possible that this difference is due, at least in part, to the fact that both of those investigations dealt with quasiplane jets without sidewalls and also used nozzles with different contraction profiles. Figure 20 also shows that $\mathrm{St}_{\mathrm{sym}}$ is nearly independent of Re_h when $\mathrm{Re}_h \leq 10\,000$.

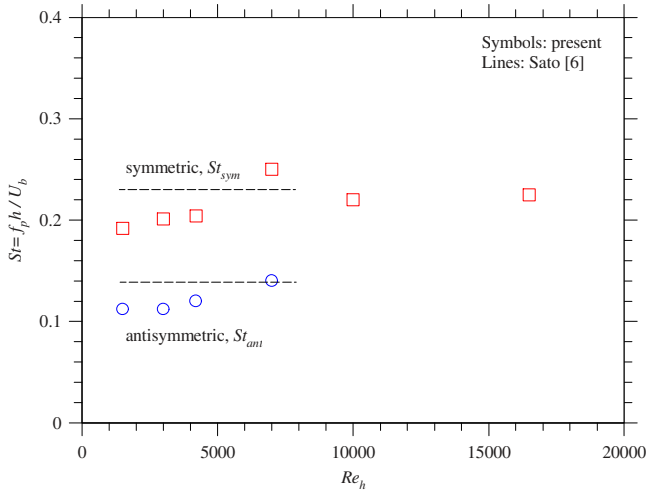

FIG. 20. (Color online) Dependence of the Strouhal number ($\mathrm{St} \equiv f_p h / U_b$) of the symmetric ($\mathrm{St}_{\mathrm{sym}}$) and antisymmetric ($\mathrm{St}_{\mathrm{ant}}$) modes on Re_h. Note that the values of $\mathrm{St}_{\mathrm{sym}}$ and $\mathrm{St}_{\mathrm{ant}}$ are those of f^* corresponding to peaks of Φ_u between $x/h=2$ and $x/h=6$ as indicated in Fig. 19 by dashed lines.

Now we examine the far-field u-spectra Φ_u and their centerline evolution. Figures 21(a)–21(d) present the far-field data of Φ_u obtained at $x/h=20$, 40, and 80 on the centerline in the form of $f\Phi_u$ versus $\log(f y_{0.5}/U_c)$ to identify the peak of Φ_u due to the presence of the far-field coherent structures and their quasiperiodic passage.[50] Note that the results for $\mathrm{Re}_h = 1500$ were not reliable due to too few data points of Φ_u at low frequencies ($f^* < 0.1$) even for $x/h=20$ and are thus not reported here. Note that this corresponds to the product of a local Strouhal number and the frequency, in contrast to the exit Strouhal number reported earlier. It is evident that the spectral peak of the turbulent kinetic energy is centered around $f_p^* = f_p y_{0.5}/U_c \approx 0.1$ to 0.22 (depending on Re_h). We also estimated the results of Φ_u at $y_{0.5}$ from measurements of u across the jets. Figure 22 shows the results for $\mathrm{Re}_h = 16\,500$. It is demonstrated by the dashed lines of Figs. 21(c) and 22 that the value of f_p^* for $y=y_{0.5}$ is about a half of the centerline value. This is consistent with previous findings that the far-field vortex structures are antisymmetrically located on either side of the centerline of a plane jet,[50–53] so that the local structural frequency recorded on the centerline should be twice that obtained at $y=y_{0.5}$ or beyond. The same finding was also observed by Thomas and Prakash.[50] It follows that the local passage normalized frequency of the vortical structures should be $[f_p^*]_{\mathrm{true}} = 0.5[f_p^*]_{\mathrm{CL}}$. Figure 23 shows the present result of $[f_p^*]_{\mathrm{true}}$ versus Re_h, together with those previously reported in Refs. 50–53. Note that the relation $[f_p^*]_{\mathrm{true}} = 0.5[f_p^*]_{\mathrm{CL}}$ was used to determine the value of $[f_p^*]_{\mathrm{true}}$ for Antonia *et al.*[51] since their measurements only provided $[f_p^*]_{\mathrm{CL}}$ (see their Fig. 2).

Figure 23 demonstrates that the normalized frequency $[f_p^*]_{\mathrm{true}}$ increases noticeably with Re_h. This Re_h dependence is consistent with the near-field result of Fig. 20. This observation, based on both the present and previous measurements, does not support the claim of Cervantes de Gortari

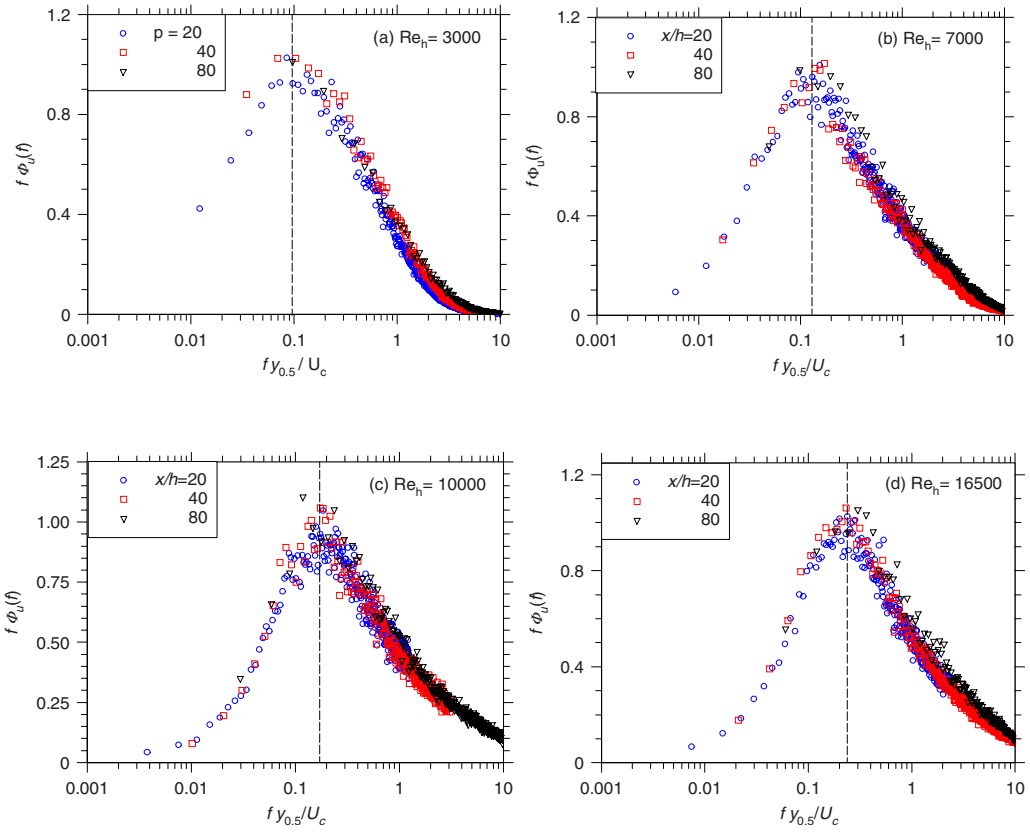

FIG. 21. (Color online) Evolution of the centerline Φ_u obtained at $x/h=20$, 40, and 80 in the form of $f\Phi_u$ vs $\log(fy0.5/U_c)$.

and Goldschmidt[52] that $[f_p^*]_{\text{true}}(\approx 0.11)$ is independent of the Reynolds number in the range of their investigation, i.e., $\text{Re}_h=7900-15\,100$ (see Fig. 23). The suggestion of these authors that the apparent "flapping" is a universal feature of the plane jet, i.e., caused by a bulk displacement of the mean velocity profile, is also ruled out by, e.g., Antonia *et al.*[51] The flapping is actually associated with the quasiperiodic passage of the far-field coherent structures.

B. Interpretation of differences in statistical properties due to varying Re_h

It is evident from the above analysis that, in the near-field region, the arrays of the vortical structures in the mixing layers on either side of the $\text{Re}_h=1500$ jet can exhibit either the symmetrical or the antisymmetrical modes of motion (and growth) with respect to the centerline. As Re_h is increased, the symmetric mode becomes more predominant, as evidenced by a higher passage rate of primary structures ($\text{St}_{\text{sym}} > \text{St}_{\text{ant}}$, see Fig. 20). This change in mode is associated with an increase in near-field spread and entrainment, as evi-

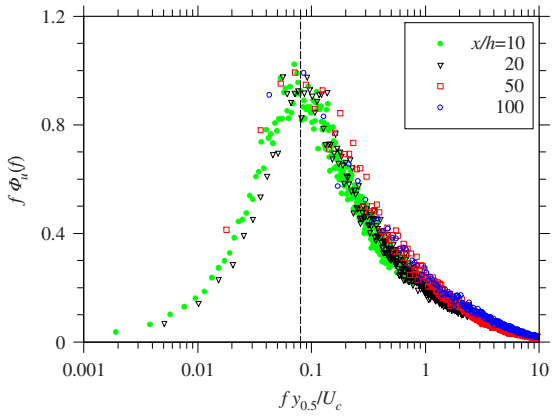

FIG. 22. (Color online) Streamwise evolution of Φ_u for $y=y_{0.5}$ obtained at $x/h=20$, 40, and 80 in the form of $f\Phi_u$ vs $\log(fy0.5/U_c)$.

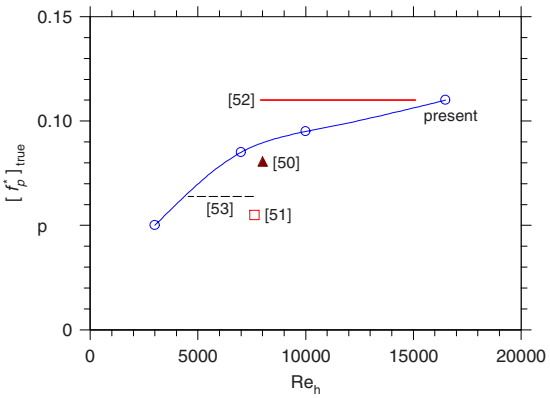

FIG. 23. (Color online) Dependence of $[f_p^*]_{\text{true}}$ on Re_h.

denced by the reduction in potential core length with increasing Re_h (Figs. 4–6). It therefore implies that the symmetric mode is more effective at entrainment in the near field than is the antisymmetric mode. This change in dominant mode type can also explain why the local maximum ($u^*_{c,max}$) of the turbulence intensity $u^*_c = u'_c/U_c$ decreases significantly with increased Re_h since the antisymmetric mode can be expected to cause higher centerline fluctuations, whereas its x-location (x^*_{max}) shifts upstream (see Fig. 12), since this peak is associated with the end of the potential core, being caused by the collision of the vortices on either side of the layer. This also can explain the Re-dependent discrepancies of variations of the near-field skewness and flatness factors of u (see Figs. 14 and 15). Furthermore, for $Re_h \geq 10\,000$, the asymmetric mode is no longer present, as evidenced by the Strouhal number St_{sym} being nearly independent of Re_h (see Fig. 20). Importantly, this is associated with no obvious Re-dependent differences in the various statistical properties being observed for $Re_h \geq 10\,000$.[54]

Next we seek an explanation for why the trends in the influence of Re_h in the near-field and far-field rates of spread and decay are opposite. The investigation of Antonia *et al.*[51] (and others) reveals that the far-field coherent structures are established at a location well downstream from the nominal merging point of the mixing layers but upstream from the onset of self-preservation. This was observed for a jet with $Re_h \approx 7700$, where the symmetric mode can be expected to dominate. It is possible that the interaction of symmetrical primary structures from the opposite mixing layers results in their own destruction when they collide near to the end of the potential core, which would require new structures to form further downstream. Since the antisymmetric mode is prevalent in the far field, this can also explain why the modes are different in the near and far fields. However, such destruction is less likely to occur for the antisymmetric mode. Furthermore, the antisymmetric mode can propagate directly into the far field, without losing as much vortical energy in the merging process of the two layers, explaining why the far-field spreading rate is higher for jets with an initially antisymmetric mode. The good match of near-field and far-field Strouhal numbers gives further support that this direct propagation at low Re_h is possible.

We also note from Fig. 23 that the scaling passage frequency of the far-field structures increases with Re_h. This implies that the effect of Re_h on the far-field organized motion is not negligible, in contrast to the constant value of $[f^*_p]_{true}$ reported earlier.[52] Significantly, for a fixed value of Re_h, the dimensionless $[f^*_p]_{true}$ is approximately constant in the self-similar region (of the mean velocity), i.e., independent of x. This means that the frequency (f_p) associated with the passage of coherent structures decreases with downstream distance (x) as $f_p \sim x^{-1.5}$, as derived from the observed relations $U_c \sim x^{-1/2}$ (Fig. 4) and $y_{0.5} \sim x$ (Fig. 9). Likewise their scale varies directly with x. Antonia *et al.*[51] estimated their size by integrating the maximum coherence between the lateral fluctuations of velocity in the y-direction and obtained that the streamwise extent of the structures is at least two to three times as large as the lateral ($\approx y_{0.5}$) and spanwise ($\approx 0.7 y_{0.5}$) extents. This suggests that the sizes of the far-field structures decrease with increasing Re_h. Nevertheless, it is recognized that the present spectral measurements are not sufficient to fully explain the Re_h dependence of the jets, and further work is required to confirm these deductions.

V. CONCLUSIONS

Previous experimental studies of a plane jet were confined to the high Reynolds number regime ($Re_h \geq 10\,000$) and mostly limited to a single Reynolds number, each with different initial and/or boundary conditions. Only the works of Namar and Ötügen[31] and Lemieux and Oosthuizen[30] offered a systematic investigation of Re_h. However, Namar and Ötügen's[31] jets were not constrained by sidewalls and did not extend into the asymptotic regime ($1000 \leq Re_h \leq 7000$), while that of Lemieux and Oosthuizen[30] spanned an even more limited range, $700 \leq Re_h \leq 4200$. The recent DNS of a plane jet by Klein *et al.*[33] was similarly limited in their range of Reynolds number $Re_h \leq 6000$ and axial extent $x/h \leq 20$. Accordingly, the effects of Reynolds number on a two-dimensional plane jet cannot be adequately assessed from the existing literature.

The present measurements have found the present plane jet to depend on Re_h over the range $Re_h \leq 25\,000$. Within this range, changes within both the near and far fields are found in the mean velocity decay rate and half-width, and in the evolution of turbulence intensity and skewness and flatness factors of the fluctuating velocity (u). These changes are associated with differences in the exit velocity profiles and in the frequency spectra, implying different behaviors of the underlying coherent structures. More specifically, the main findings of the influences of Re_h over this range are summarized as follows.

(1) The details of exit flows, measured at $x/h = 0.5$, depend on Re_h, although the mean velocity profiles closely approximate a top hat in each case. The lateral extent of uniform flow widens, and the thickness of exit boundary layer decreases as Re_h is increased. This is associated with a reduction in the turbulence intensity profiles there. These differences decrease asymptotically to become small, but not insignificant, for $Re_h = 10\,000$.
(2) An increase in Re_h causes the length of the potential core to decrease and the near-field spreading rate to increase. It also causes a decrease in the magnitude of the near-field hump in the streamwise distribution of turbulence intensity, $u'_{c,max}$, and also in its axial location from $x_{c,max} \approx 18h$ to $10h$.
(3) Over the range $1500 \leq Re_h < 10\,000$, the near-field, primary coherent structures are found by spectral analysis to occur bimodally in both the symmetric and antisymmetric modes with respect to the jet centerline. While the symmetric mode dominates at $Re_h = 1500$, the prevalence of the antisymmetric mode increases with Re_h to become dominant at $Re_h \geq 10\,000$. The corresponding Strouhal numbers are found to increase slightly, but discernibly, with increasing Re_h. It is found that the symmetric mode results in higher rates of near-field entrainment and growth than does the antisymmetric mode.

(4) Secondary coherent structures are present in the far field and their passage frequency (f_p) follows the relation $f_p \sim x^{-1.5}$, as shown in previous studies. The characteristic size of these structures thus obeys the requirement for self-preservation. It is the new finding of the present work that the local Strouhal number $\mathrm{St}=f_p y_{0.5}/U_c$ varies between 0.05 and 0.11 when Re_h is varied from 1500 to 16 500 (Fig. 23). This finding differs from the previous claim that St=0.11 independent of the magnitude of Re_h.[52]

(5) The far-field rates of mean velocity decay and spread exhibit the opposite dependence on Re_h to the near field. That is, they decrease asymptotically as Re_h is increased. Their rates of asymptotic convergence are comparable with that in the near field.

(6) The underlying structure in the far field is confirmed to be in the antisymmetric mode, as found previously.[50–52] It is hypothesized that the opposite trend in spreading rates in the near and far field (above) may be caused by the cancellation of much more of the coherent motions for the symmetric mode than for the antisymmetric mode when the coherent motions collide near the end of the potential core. That is, some of the near-field antisymmetric vortices can propagate directly into the far field, while the symmetric vortices largely cancel and must re-establish in the antisymmetric mode.

(7) The local Reynolds number, $\mathrm{Re}_{y0.5} \equiv 2U_c y_{0.5}/\nu$, is found to increase with downstream distance as $\mathrm{Re}_{y0.5} \sim x^{1/2}$, for all cases of investigation, and this scaling begins almost immediately downstream from the end of the potential core. This implies that all jets must eventually attain a high $\mathrm{Re}_{y0.5}$ no matter how low is the initial Re_h. Nevertheless, each jet converges to a different asymptotic state.

(8) In the self-similar field, the asymptotic value of streamwise turbulence intensity increases with an increase in Re_h, as do the asymptotic values of the skewness and flatness factors.

(9) For $\mathrm{Re}_h \geq 1500$, both self-preserving relations of the kinetic energy dissipation (ε) and Kolmogorov scale (η), i.e., $\varepsilon \sim \mathrm{Re}_h^3 (x/h)^{-5/2}$ and $\eta \sim \mathrm{Re}_h^{-3/4} (x/h)^{5/8}$, become valid from $x/h=20$, a location, which is significantly closer to the jet exit than those required for achieving the asymptotic values of the turbulence intensity, the skewness, and flatness factors of u.

ACKNOWLEDGMENTS

The authors gratefully acknowledge the support of the Fluid Mechanics, Energy and Combustion Group of The University of Adelaide, the Endeavor Postgraduate Research Scholarship, and ARC Linkage Scheme. We are thankful to Professor W. K. George (Chalmers University of Technology) for insightful comments on R.C.D.'s doctoral thesis, particularly of discussions on the local Reynolds number effect. Finally, we thank the reviewers for insightful comments, which have strengthened the final draft of this manuscript.

[1] H. Schlichting, "Laminare strahlausbreitung," ZAMM **13**, 260 (1933).
[2] E. Forthmann, "Über turbulente strahlausbreitung," Ing.-Arch. **5**, 42 (1934) [translated as "Turbulent jet expansion," National Advisory Committee for Aeronautics Technical Memorandum No. 789, National Aeronautics and Space Administration (1936)].
[3] W. Bickley, "The plane jet," Philos. Mag. **23**, 727 (1937).
[4] D. R. Miller and E. W. Comings, "Static pressure distribution in a free turbulent jet," J. Fluid Mech. **3**, 1 (1957).
[5] B. G. Van Der Hegge Zijnen, "Measurements of the distribution of heat and matter in a plane turbulent jet of air," Appl. Sci. Res., Sect. A **7**, 277 (1958).
[6] H. Sato, "The stability and transition of a two-dimensional jet," J. Fluid Mech. **7**, 53 (1960).
[7] G. Heskestad, "Hot-wire measurements in a plane turbulent jet," ASME Trans. J. Appl. Mech. **32**, 721 (1965).
[8] L. J. S. Bradbury, "The structure of self-preserving turbulent planar jet," J. Fluid Mech. **23**, 31 (1965).
[9] P. E. Jenkins and V. W. Goldschmidt, "Mean temperature and velocity measurements in a plane turbulent jet," ASME Trans. J. Fluids Eng. **95**, 581 (1973).
[10] E. Gutmark and I. Wyngnanski, "The planar turbulent jet," J. Fluid Mech. **73**, 465 (1976).
[11] R. C. Deo, J. Mi, and G. J. Nathan, "The influence of nozzle aspect ratio on a plane jet," Exp. Therm. Fluid Sci. **31**, 825 (2007).
[12] W. K. George, *Recent Advances in Turbulence* (Hemisphere, New York, 1989), pp. 39–73.
[13] P. Bradshaw, "Effects of external disturbances on the spreading rate of a plane turbulent jet," J. Fluid Mech. **80**, 795 (1977).
[14] J. Mi, D. S. Nobes, and G. J. Nathan, "Influence of jet exit conditions on the passive scalar field of an axisymmetric free jet," J. Fluid Mech. **432**, 91 (2001).
[15] R. C. Deo, "Experimental investigations of the influence of Reynolds number and boundary conditions on a plane air jet," Ph.D. thesis, The University of Adelaide, Australia, 2005. Available at Australian Digital Thesis Program, http://thesis.library.adelaide.edu.au/public/adt-SUA20051025.054550/index.html.
[16] R. C. Deo, J. Mi, and G. J. Nathan, "The influence of nozzle-exit geometric profile on statistical properties of a turbulent plane jet," Exp. Therm. Fluid Sci. **32**, 545 (2007).
[17] R. C. Deo, J. Mi, and G. J. Nathan, "Comparison of turbulent jets issuing from rectangular nozzles with and without sidewalls," Exp. Therm. Fluid Sci. **32**, 596 (2007).
[18] K. B. M. Q. Zaman, "Far-field noise of a subsonic jet under controlled excitation," J. Fluid Mech. **152**, 83 (1985).
[19] N. R. Panchapakesan and J. L. Lumley, "Turbulence measurements in axisymmetric jets of air and helium, Part 1, air jet," J. Fluid Mech. **246**, 197 (1993).
[20] H. J. Hussein, S. P. Capp, and W. K. George, "Velocity measurements in a high Reynolds number momentum conserving axisymmetric turbulent jet," J. Fluid Mech. **258**, 31 (1994).
[21] P. E. Dimotakis, "The mixing transition in turbulent flows," J. Fluid Mech. **409**, 69 (2000).
[22] P. E. Dimotakis, R. C. Miake-Lye, and D. A. Panpantoniou, "Structure and dynamics of round turbulent jets," Phys. Fluids **26**, 3185 (1983).
[23] P. L. Miller and P. E. Dimotakis, "Reynolds number dependence of scalar fluctuations in a high Schmidt number turbulent jet," Phys. Fluids A **3**, 1156 (1991).
[24] R. J. Gilbrech, "An experimental investigation of chemically reacting gas-phase turbulent jets," Ph.D. thesis, California Institute of Technology, 1991.
[25] M. M. Koochesfahani and P. E. Dimotakis, "Mixing and chemical reactions in a turbulent liquid mixing layer," J. Fluid Mech. **170**, 83 (1986).
[26] A. Michalke, "Survey on jet instability theory," Prog. Aerosp. Sci. **21**, 159 (1984).
[27] P. H. Oosthuizen, "An experimental study of low Reynolds number turbulent circular jet flow," ASME Applied Mechanics, Bioengineering and Fluids Engineering Conference, Houston, TX, 20–22 June 1983, ASME Paper No. 83-FE-36.
[28] C. Bogey and C. Bailly, "Large eddy simulations of transitional round jets: Influence of the Reynolds number on flow development and energy dissipation," Phys. Fluids **18**, 065101 (2006).
[29] W. M. Pitts, "Reynolds number effects on the mixing behavior of axisymmetric turbulent jets," Exp. Fluids **11**, 135 (1990).

[30]G. P. Lemieux and P. H. Oosthuizen, "Experimental study of behavior of planar turbulent jets at low Reynolds numbers," AIAA J. **23**, 1845 (1985).
[31]I. Namar and M. V. Ötügen, "Velocity measurements in a planar turbulent air jet at moderate Reynolds numbers," Exp. Fluids **6**, 387 (1988).
[32]K. W. Everitt and A. G. Robbins, "The development and structure of turbulent plane jets," J. Fluid Mech. **88**, 563 (1978).
[33]M. Klein, A. Sadiki, and J. Janicka, "Investigation of the influence of the Reynolds number on a plane jet using direct numerical simulation," Int. J. Heat Fluid Flow **24**, 785 (2003).
[34]L. W. B. Browne, R. A. Antonia, S. Rajagopalan, and A. J. Chambers, "The interaction region of a turbulent plane jet," in Structure of Complex Turbulent Shear Flows, IUTAM Symposium, Marseille, 1982, pp. 411–419.
[35]F. O. Thomas and V. W. Goldschmidt, "Structural characteristics of a developing turbulent planar jet," J. Fluid Mech. **163**, 227 (1986).
[36]A. K. M. F. Hussain and A. R. Clark, "Upstream influence on the near field of a planar turbulent jet," Phys. Fluids **20**, 1416 (1977).
[37]J. Tan-Atichat, W. K. George, and S. Woodward, *Handbook of Fluids and Fluids Engineering*, edited by A. Fuhs (Wiley, New York, 1996), Vol. 3, Sec. 15.15, pp. 1098–1116.
[38]F. H. Champagne, "The fine-scale structure of the turbulent velocity field," J. Fluid Mech. **86**, 67 (1978).
[39]S. J. Kwon and I. W. Seo, "Reynolds number effects on the behavior of a non-buoyant round jet," Exp. Fluids **38**, 801 (2005).
[40]P. V. Johansson and W. K. George, "Equilibrium similarity, effects of initial conditions and local Reynolds number on the axisymmetric wake," Phys. Fluids **15**, 603 (2003).
[41]H. Tennekes and J. L. Lumley, *A First Course in Turbulence* (MIT Press, Cambridge, MA, 1972).
[42]R. A. Antonia, B. R. Satyaprakash, and A. K. M. F. Hussain, "Measurements of dissipation rate and some other characteristics of turbulent plane and circular jets," Phys. Fluids **23**, 695 (1981).
[43]J. Mi and G. J. Nathan, "The influence of probe resolution on the measurements of a passive scalar and its derivatives," Exp. Fluids **34**, 687 (2003).
[44]R. A. Antonia and J. Mi, "Corrections for velocity and temperature derivatives in turbulent flows," Exp. Fluids **14**, 203 (1993).
[45]J. Mi, R. C. Deo, and G. J. Nathan, "Fast-convergent iterative scheme for filtering velocity signals and finding Kolmogorov scales," Phys. Rev. E **71**, 066304 (2005).
[46]I. Wygnanski and E. Gutmark, "Lateral motion of the two-dimensional jet boundaries," Phys. Fluids **14**, 1309 (1971).
[47]G. S. Beavers and T. A. Wilson, "Vortex growth in jets," J. Fluid Mech. **44**, 97 (1970).
[48]D. O. Rockwell and W. O. Niccolls, "Natural breakdown of planar jets," ASME J. Basic Eng. **94**, 720 (1972).
[49]F. O. Thomas and V. W. Goldschmidt, "Structural characteristics of developing turbulent plane jets," J. Fluid Mech. **163**, 227 (1986).
[50]F. O. Thomas and K. M. K. Prakash, "An experimental investigation of the natural transition of an untuned plananr jet," Phys. Fluids A **3**, 90 (1991).
[51]R. A. Antonia, W. B. Browne, S. Rajagopalan, and A. J. Chambers, "On organized motion of a turbulent planar jet," J. Fluid Mech. **134**, 49 (1983).
[52]J. Cervantes de Gortari and V. W. Goldschmidt, "The apparent flapping motion of a turbulent plane jet—further experimental results," ASME Trans. J. Fluids Eng. **103**, 119 (1981).
[53]V. W. Goldschmidt and P. Bradshaw, "Flapping of a plane jet," Phys. Fluids **16**, 354 (1973).
[54]J. Mi, R. C. Deo, and G. J. Nathan, "Characterization of turbulent jets from high-aspect-ratio rectangular nozzles," Phys. Fluids **17**, 068102 (2005).